Visual Abstract

Numerical analysis of the crack growth path in the cement of hip spacers

Sahnoun Zengah
Department of Mechanical Engineering, Faculty of Science and Technology, University of Mustafa Stambouli, Mascara, Algeria
LPQ3M Laboratory, Faculty of Science and Technology, University of Mustafa Stambouli, Mascara, 2900, Algeria
s.zengah@univ-mascara.dz,

Abdeljelil Mankour, Sahli Abderahmane, Hichem Salah, Abdelhafid Mallek,
LMPM, Department of Mechanical Engineering, University of SidiBel Abbes, 22000, Algeria
ASAL, Centre de Développement des Satellites (CDS), Bir El Djir Oran 31130, Algeria
bm_abdeldjalil@yahoo.fr, csahliabderahmen@yahoo.fr, dsalah.hichem46@gmail.com, hafid_22@yahoo.fr,

Mohammed Mokhtar Bouziane
Department of Mechanical Engineering, Faculty of Science and Technology, University of Mustafa Stambouli, Mascara, Algeria
LMPM, Department of Mechanical Engineering, University of SidiBel Abbes, 22000, Algeria
m.bouziane@univ-mascara.dz

ABSTRACT. The use of temporary hip prosthesis made of orthopedic cement (spacer) in conjunction with antibiotics became a prevalent method used for prosthetic infections remedy; consequently, this method makes bone cement (PMMA) more fragile. Hence, the necessity of reinforcement incorporation is crucial to strengthen the bone cement. In this study, the finite element (FE) method was used to analyze the spacers behavior. FE model using an implicit integration method was used to simulate the mechanical behavior of the spacer under static loading. In addition, the extended finite element method (XFEM) was also used to investigate the fracture behavior of the non-reinforced and reinforced spacers. The results of this numerical analysis showed that the simulated crack initiation and propagation were in a good accordance with in vivo radiography and in vitro experimental observations. The full-stem reinforcement of 8 mm using reduce significantly the stress intensity factor and, consequently prevent the spacer fracture effectively. The FE models developed in this study contribute to help mechanical designers and engineers for prostheses' quality and durability improvement.

KEYWORDS. Biomechanics; Hip Spacer; Bone Cement; Fracture; XFEM.

OPEN ACCESS

Citation: Zengah, S,. Mankour, A,. Sahli, A,. Salah, H,. Mallek, A.,. Bouziane, M.M., Numerical Analysis of the Crack Growth Path in the Cement of Hip Spacers, Frattura ed Integrità Strutturale, 61 (2022) 266-281.

Received: 31.03.2022
Accepted: 24.05.2022
Online first: 31.05.2022
Published: 01.07.2022

INTRODUCTION

Prosthetic surgery is a complex intervention with major per and post-operative risks, hence, infection of joint prosthesis is a frequent complication occurring about nearly 2.5% of implanted patients which is considered one of the most difficult issue to manage [1]. The infection management regarding THA must be planned the earliest; therefore, recovery in two stages remains the reference, its purpose reposes on infection eradication and preserves the function of the joint. The principle of this intervention is based on the removal then cleaning of the infected prosthesis and insertion of a temporary prosthesis "spacer" made of orthopedic cement [2-3]; the spacer will remain in place for several weeks permitting the infection heals; subsequently, the second operation will be performed by replacing the spacer with the final prosthesis. The spacer is enriched with antibiotics which will allow the infection treatment with very high local doses of antibiotics. Commercial models of cement hip spacer can be improved by the addition of a hard reinforcement composed of an inert (non-reactive) material having a very high tensile strength to withstand the forces imposed by the human body weight [4].As the strength of the cement material is limited, Thielen et al. tested the mechanical strength of PMMA for spacer without reinforcement (Fig. 1 (a)),the second reinforced with a rod titanium reinforcement (Fig. 1 (b)) and the last one containing a full-stem titanium (Fig. 1 (c)) [5]. This spacer has been the subject of some numerical studies [6,7] in which the authors have analyzed its behavior under static loading; Salah et al. performed a parametric optimization of the reinforcement [8] and Mallek et al. studied its failure under quasi-static loading [9]. The objective of this numerical analysis is to choose among the reinforcements currently available the one allowing improving the biomechanical behavior of the hip spacer (resistance of the spacer and the reinforcement but also behavior of the bone with respect to the absorbed constraints)

The XFEM method makes it possible to predict the seat of crack initiation in the PMMA independently of the mesh chosen [7,9], and then the classical finite element method in association with the submodel technic allows the analysis of mode of crack propagation in the different types of hip spacer.

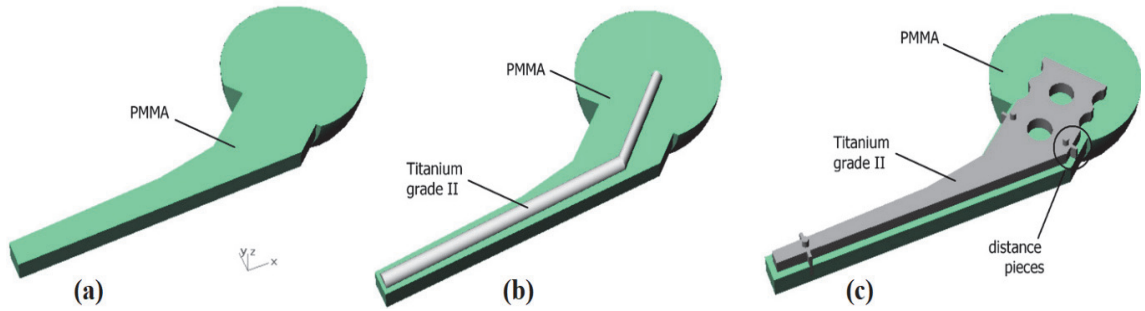

Figure 1: Different spacer types: (a) non-reinforced spacer out of PMMA; (b) rod reinforced spacer out of PMMA with a central rod pin out of titanium grade two; (c) full-stem reinforced spacer out of PMMA with a titanium grade endoskeleton [5]

MATERIAL

The spacer model adopted for the analysis consists of the assembly of four parts: cortical bone, cancellous bone, cement and reinforcement (rod reinforcement and full-stem reinforcement). The model was created by SolidWorks software and then exported in the ABAQUS finite element code. Using SOLIDWORKS facilitate the conception, and different parts assembly of 3D hip spacer model; also, give as the ability of design modification with minimum time.

Mesh and mechanical properties

ABAQUS solver was used for pre and post-processing of hip spacers model. Hence, the model components were meshed using quadratic tetrahedral elements with ten nodes (C3D10). Quadratic tetrahedral elements allow to mesh complex geometries efficiently (femoral bone), on other hand permits a significant distortion of the elements and represents stress concentrations effectively especially in the case of models dominated by bending [10]. A refinement of the mesh was generated around the prosthesis, (Fig. 2), a mesh size of 1mm lead to satisfy the convergence tests requirement. The convergence of mesh was conducted in which a sequence of numerical analysis was treated with fixed boundary

conditions. Therefore, convergence was accomplished when the refined model gives a constant result with less than 4 % change between successively improvement mesh dimensions.

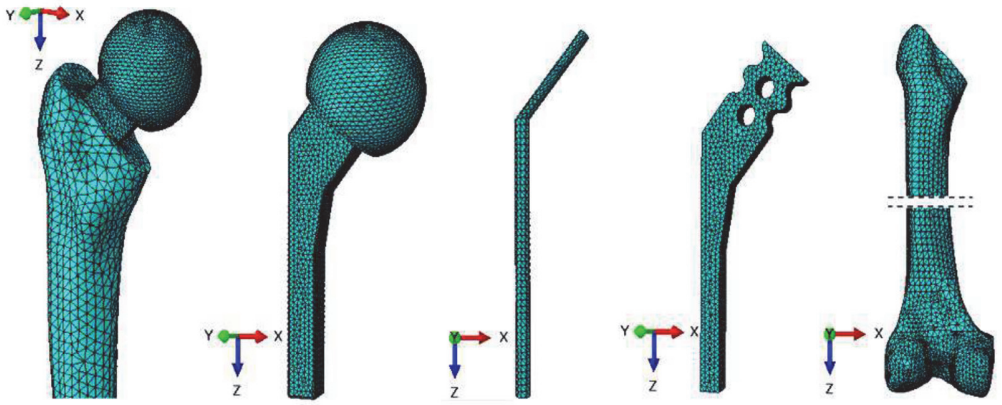

Figure 2: Finite element meshes of hip prosthesis components: hip spacer, implant spacer, rod reinforcement ,full-stem reinforcement, and femur bone (from left to right).

The mechanical properties of components material (Tab. 1) were defined as a function of Young's modulus and Poisson's ratio for cement, bone and all associated components. All materials are considered to have homogeneous isotropic and elastic behavior.

Materials	Young Modulus (MPa)	Poisson ratio
Cortical bone	15500	0.28
Concelleous bone	389	0.3
Titanium (Ti-6Al4V)	110000	0.3
Bone cement (PMMA)	2700	0.35

Table1: Mechanical properties of materials [8,19].

Boundary conditions and statics loads

In this study, the magnitude and directions of muscle forces given by Bergmann [11] were applied. Forces details are shown in Tab. 2; the static load represents the body weight of 70 kg. An abductor muscle (F abductor muscle) is applied on the proximal area.

Load (N)	X	Y	Z
Joint contact force (F_{static})	-433.8	-263.8	-1841.3
Abductor muscle	465.9	34.5	695
Vastus Lateralis	-7.2	-148.6	-746.3

Table 2: Applied forces details [11].

The tibialis muscle load (Filio-tibial tract) was applied on the lower part of the femur along the longitudinal direction of the femur [11]. The boundary condition was applied by fixing the epiphysis (Fig. 3), which represents the distal end of the femur connected to the knee joint [12]. According to Nuño et al., the overall range of the mean coefficients of friction varied between 0.17 and 0.32 in dry or wet conditions between Ti-6Al-4V and PMMA in defining the interface conditions for finite element analysis and design of cemented hip implants. The choice of using surface-to-surface contact is the only possible approach when using tetrahedral elements with a friction coefficient of 0.25 [13].

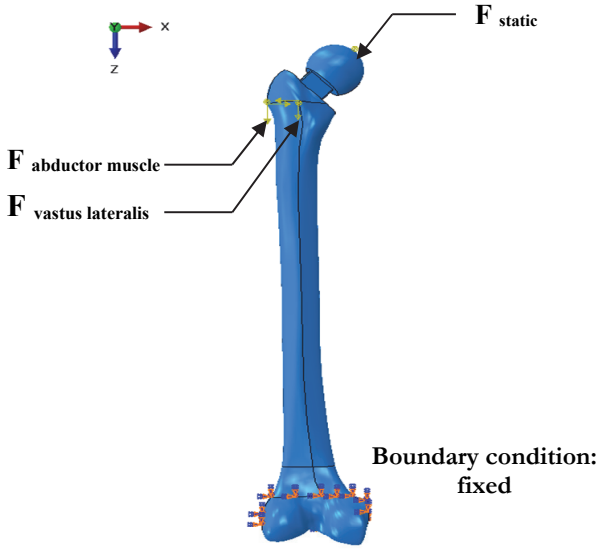

Figure 3: Boundary condition and acted forces on the model [11]

METHOD

XFEM rupture Criterion

The extended finite element method is an extension of the classical FEM finite element method, in the case of the presence of discontinuities in the studied space. The involvement of this method allows to model the transition from damage to fracture by improving an existing mesh with shape functions able to representing discontinuities in areas and gradients in addition to singularities [14]. The classical finite element method is unable to reproduce a discontinuity with good precision since the shape functions are constructed with a polynomial basis. In an XFEM method, the discretization is done first in classical FEM far from the discontinuity, then the enrichment is introduced at the level of the discontinuity using news shapes functions (equ.1).

$$u(x) = u^{FEM} + u^{Enrich} = \sum_{I=1}^{N} N_I(x)\left[u_I + H(x)q_I + \sum_{\alpha=1}^{4} F_\alpha(x)b_I^\alpha\right] \tag{1}$$

where $N_I(x)$ is the finite element shape function, q_I is the enriched nodal degree of freedom vector associated with the discontinuous jump function H(x) through the crack surfaces. b_I^α, represents the vector of degree of freedom enriched in crack tip, and Fα (x) is the asymptotic function associated with the elastic crack tip.
For an element completely cut by a crack, the Heaviside enrichment function is used such that

$$H(x) = \begin{cases} +1 & \textit{above the crack} \\ -1 & \textit{below the crack} \end{cases} \tag{2}$$

In the case of an element containing the crack tip, the asymptotic functions describing the displacement field close to the tip take the form of the four following functions:

$$\{F_\alpha(x)\}_{\alpha=1-4} = \left\{\sqrt{r}\sin\frac{\theta}{2}, \sqrt{r}\cos\frac{\theta}{2}, \sqrt{r}\sin\theta\sin\frac{\theta}{2}, \sqrt{r}\sin\theta\cos\frac{\theta}{2}\right\} \tag{3}$$

where r and θ are the polar coordinates in the local coordinate system of the crack tip, with its origin at the crack tip and θ = 0 is tangent to the crack tip. In ABAQUS the XFEM gives to the crack a cohesive behavior, by using the phantom node method (Fig. 4). This allow to model crack initiation and propagation in any arbitrary path, thus exploiting the advantages of the XFEM and cohesive zone methods [15]. In this case, the asymptotic singularity was replaced by a cohesive zone and only the displacement progression through a completely cracked element was considered [16].
The cohesive zone model used in this study is based on the continuum damage mechanics theories [29, 30]. PMMA is modelled as a quasi-brittle material with a cohesive zone at the crack tip. The ABAQUS cohesive element material law is described by the shape of triangle, and thus definition of G_c alone is not sufficient. Critical release energy is related to cohesive material's effective ultimate nominal stress, T_{ult}, and cohesive ductility (failure separation), δf via

$$G_c = \frac{T_{ult}\delta^f}{2} \tag{4}$$

The implant-cement interfacial behaviour was described by an initial elastic behaviour followed by the initiation and the evolution of damage. The damage variable D at the cement-implant interface was defined by this equation:

$$\mathrm{D} = \int_{\delta_m^0}^{\delta_m^f} \frac{T_{eff}\, d_\delta}{G_c - G_0} \tag{5}$$

where T_{eff} and δ are the effective traction and displacement, respectively, δ_m^f and δ_m^0 are displacements at the fracture and damage initiation, respectively. $G_c$and G_0 are the fracture energy and elastic energy at damage initiation, respectively. The constitutive relationship of the entire interfacial behaviour may be expressed as:

$$\begin{cases} K_{0i}\delta_{0i} \; if \; \delta_i \le \delta_{0i} \\ (1-D)K_{0i}\delta_{0i}\delta_i < \delta_{0i} < \delta_{0C} \\ 0 \qquad\qquad if \delta_{0i} \ge \delta_{0C} \end{cases} \tag{6}$$

where, in shear direction i, K_{0i} is the initial stiffness, δ_{0i} is the maximum relative displacement in the linear region and δ_{Ci} is the critical displacement at fracture.

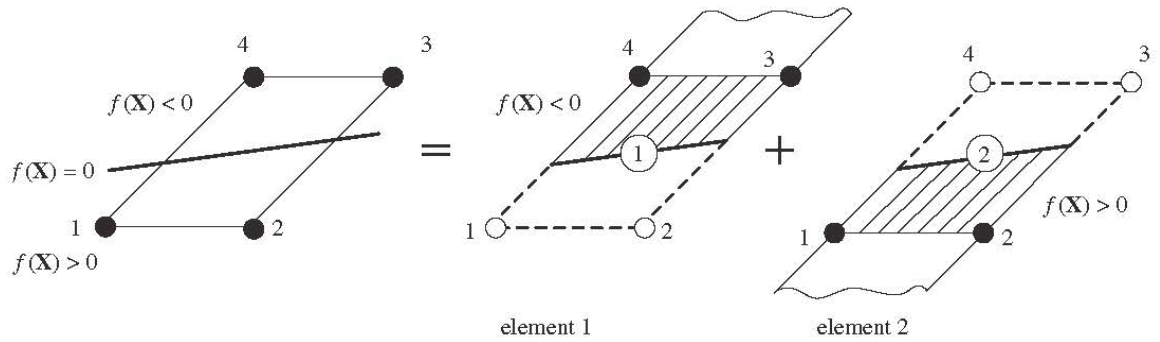

Figure 4: Principal of the phantom node method: decomposition of a cracked element into two elements; filled circles represent real nodes and empty circles phantom nodes. Each real node remains connected to the corresponding phantom node until the ultimate tensile force is exceeded [15].

The crack initiation represents the beginning of cohesive response degradation at the level of an enriched element. The degradation process initiates when the stresses or strains meet the specified crack initiation criteria. The maximum principal stress criterion is used which can be represented as:

$$\mathrm{f} = \left\{ \frac{\sigma_{\max}}{\sigma_{\max}^0} \right\} \tag{7}$$

where σ_{max}^{0} represents the maximum principal stress that can be supported by the material. The Macaulay brackets <> indicates that pure compressive stresses do not cause crack initiation. The damage initiated when the ratio (equ.4) reaches unity value [10].
The initiation of crack occurs when the maximum principal stress exceeds the tensile failure limit of the orthopedic cement (35 MPa [17]), and the modeling of the crack propagation is described by the intermediary of the PMMA fracture energy (400 J/m²) [18].

Stress intensity factor (SIF) calculations

The main object of this work focuses on the analysis of a crack behavior initiated within orthopedic cement spacer, which permit to predict the risk of rupture. Hence, this risk will be analyzed reposing on the variations of stress intensity factors in mode I and shear modes (II and III). To achieve this purpose, a semi-elliptical crack (Fig. 5) is placed in the left posterior edge of the spacer, just above its insertion into the femur. The selected region presents the most favorable risk of rupture.

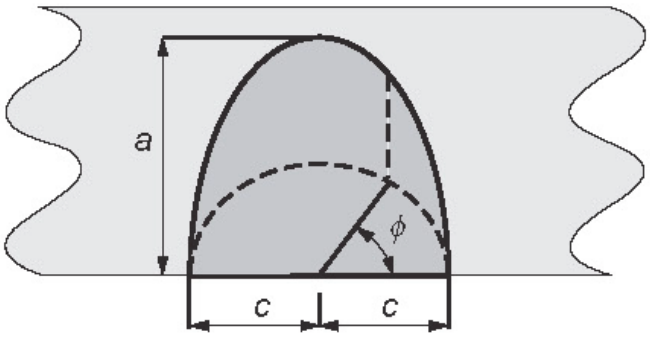

Figure 5: Radius characteristic of a semi-elliptical crack

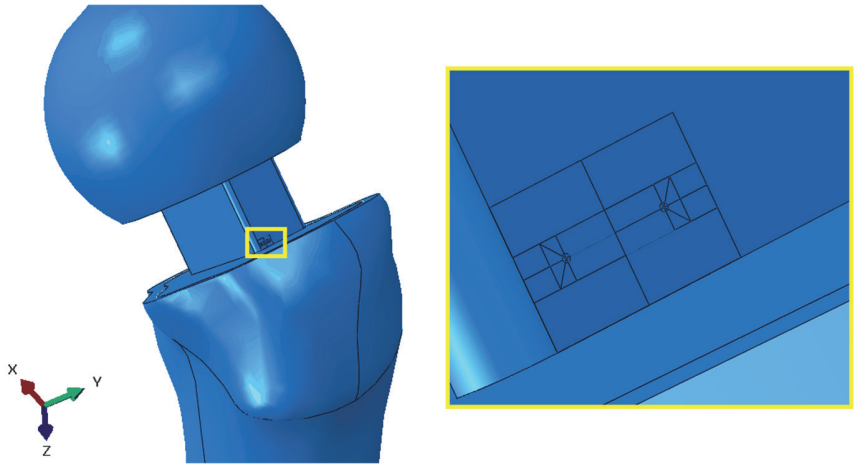

Figure 6: Sub-model placed in the spacer left edge above the insertion into the bone

Several cracks were created of which the large radius "a" is equal to 1mm and the small radius "c" varies from 0.2 to 1mm by a step of 0.2 mm (Fig. 5). The stress intensity factor will be calculated in the contours around the nodes of the crack front whose positions are expressed in standard distance, 0 being the end of the left edge side (Fig. 6).
Although the XFEM method makes it possible to calculate the SIF for a crack under mixed-mode loading without modifying the mesh, however the results present oscillations and the convergence is sometimes difficult [19], for this we have used the interaction integral method, this method uses auxiliary fields (stresses or strains around the crack tip) superimposed on top of the actual fields [20]. Qian, G., et al. demonstrated that this method is appropriate to determine accurate K values for 3D cracks [19]. By associating the interaction integral method with the Sub-modeling technique (Fig. 6) the computation can be accelerated. This technique is based on the principle of St. Venant [21], the results of the analysis made on the coarsely meshed global model serve as boundary conditions for the finely meshed sub-model with

quadratic hexahedral elements C3D20, a particle radial mesh technique around the crack front (Fig. 7) allows to obtained an accurate result [10]. The convergence of the mesh is checked by the value of the SIF, this convergence is done from the fifth contour for a crack tip containing 40 nodes.

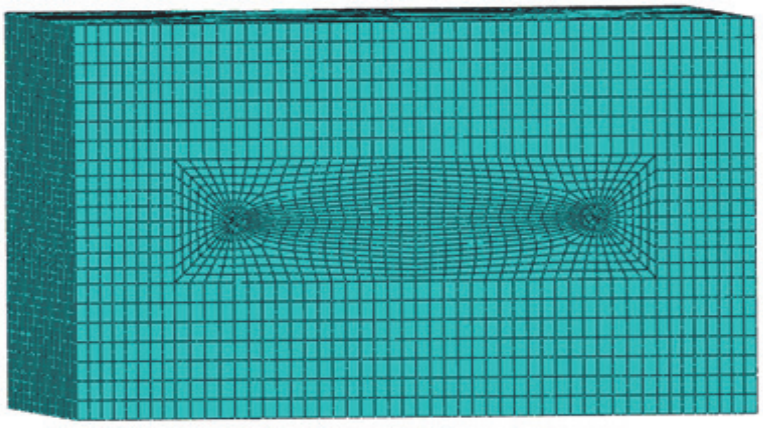

Figure 7: Finite element mesh of Sub-model.

RESULTS AND DISCUSSION

Distributions of the maximum principal stresses in the spacer

The maximum principal stress illustrates the mechanical behavior of the different spacer models; since it represents the failure criterion of several damage models dedicated to fragile materials [9, 17, 22].

The distribution of the maximum principal stress on the rear face of the spacer shows that, the stresses are positive (tensile stress), with a high concentration at two points located on the left rear edge (Fig. 8); the opposite edge is the region of the maximum compressive stress which is located just below the insert (Fig. 9). The PMMA bone cement had a weak capability to support tension and shear loading; on other hand, a superior ability to withstand compression loading [23]. The maximum principal stress exceeds 35 MPa (tensile strength) [17], in the spacer without reinforcement and with rod reinforcement. The involvement of full-stem reinforcement of8 mm reduce the stress to 21.7 MPa, which permits a reduction of 35% compared to the rod reinforcement and of more than 80% compared to the spacer without reinforcement. In order to better compare the distribution of stresses in the spacer, we assess its evolution along the rear left and front right edges subjected to maximum stresses in tension and compression respectively (Fig. 10).

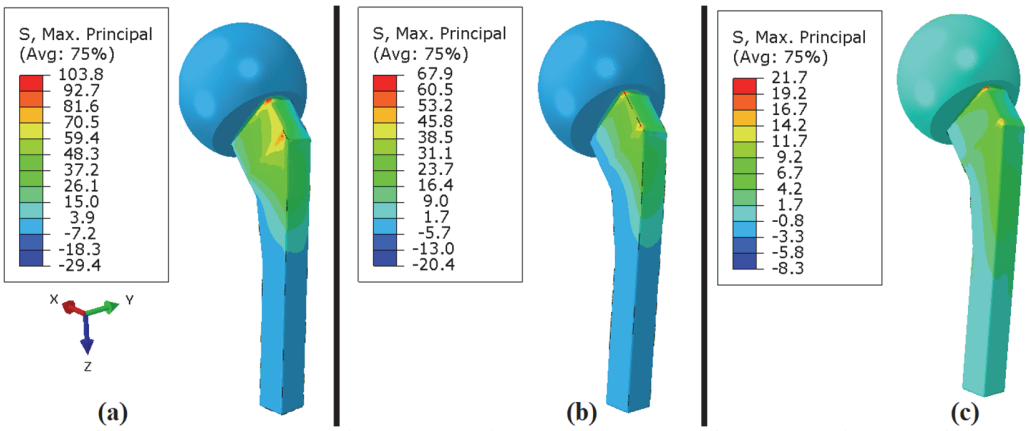

Figure 8: Distribution of the maximum principal stresses in the spacer (posterior face); (a) without reinforcement, (b) with rod reinforcement, (c) with full-stem reinforcement

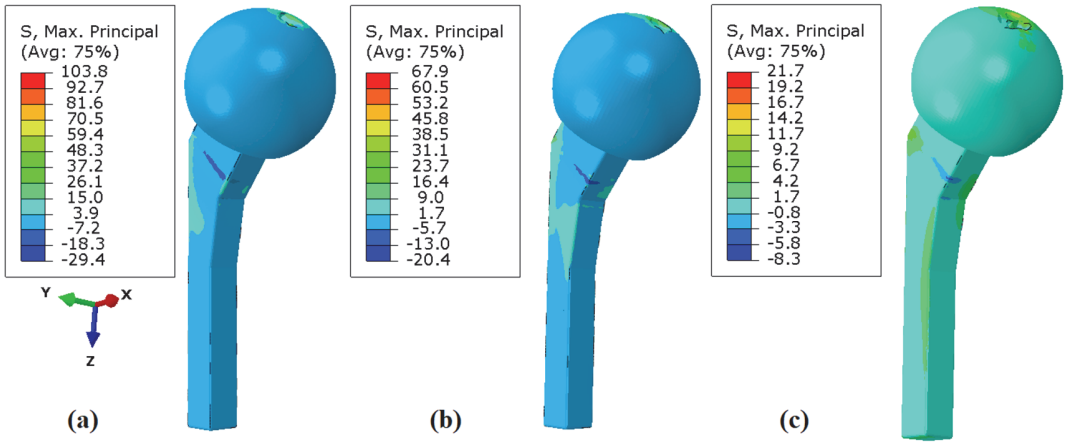

Figure 9: Distribution of the maximum principal stresses in the spacer (anterior part); (a) without reinforcement, (b) with rod reinforcement, (c) with full-stem reinforcement

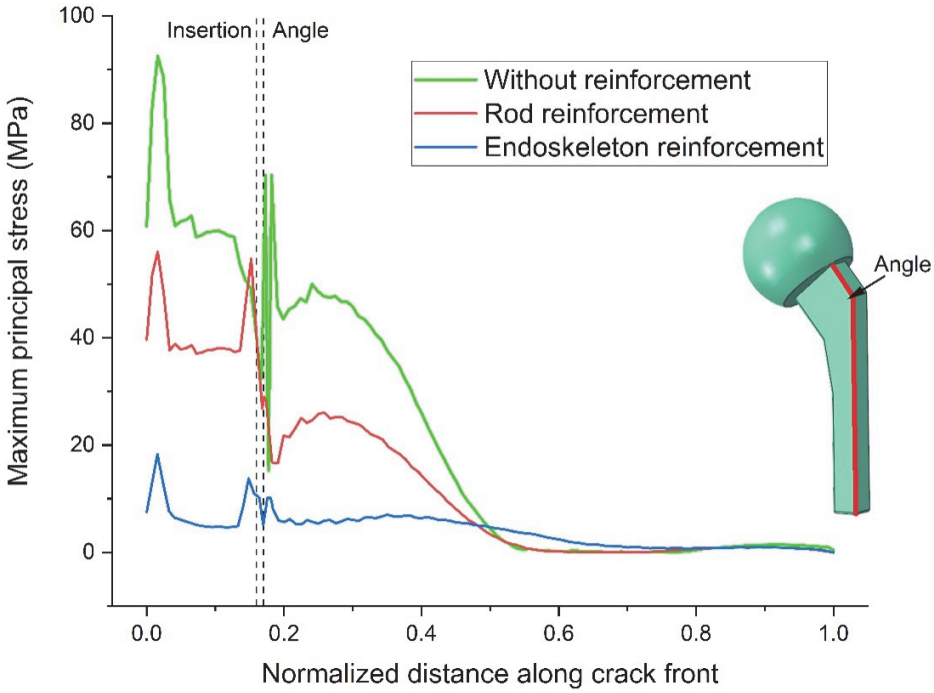

Figure 10: Distribution of the maximum principal stress at the level of the left posterior edge of the spacer

At the level of the posterior edge, the maximum principal stresses are exclusively positive, which vary considerably depending on the choice of reinforcement type. However, the overall evolution is similar with a first peak appear at the junction of the rod with the prosthetic head and a the second one was slightly less important near the spacer insertion to the bone, and the stresses were relatively constant between the two zone. regarding the spacer without reinforcement and rod reinforcement, the maximum principal stresses exceed the critical value of 35 MPa along all the parts of the rod located above the insert. The full-stem reinforcement, absorbing a large part of the forces, which allows it to be reduced considerably. Below the insertion zone, the stresses decrease significantly to almost zero at the level of the middle zone of the rod. Therefore, the behavior changes completely at the anterior edge level (Fig. 11) and the stresses oscillate among positive and negative values along the rod part located between the prosthetic head and the first angle of the anterior edge (which is located below the insertion level). The most important peak values are the compression ones located at the rod-

head junction, next to the insertion and at the first angle. Regarding the posterior edge, the stress is null beyond the middle of the rod. The use of a full-stem reinforcement allows a minimum and most stable stresses.

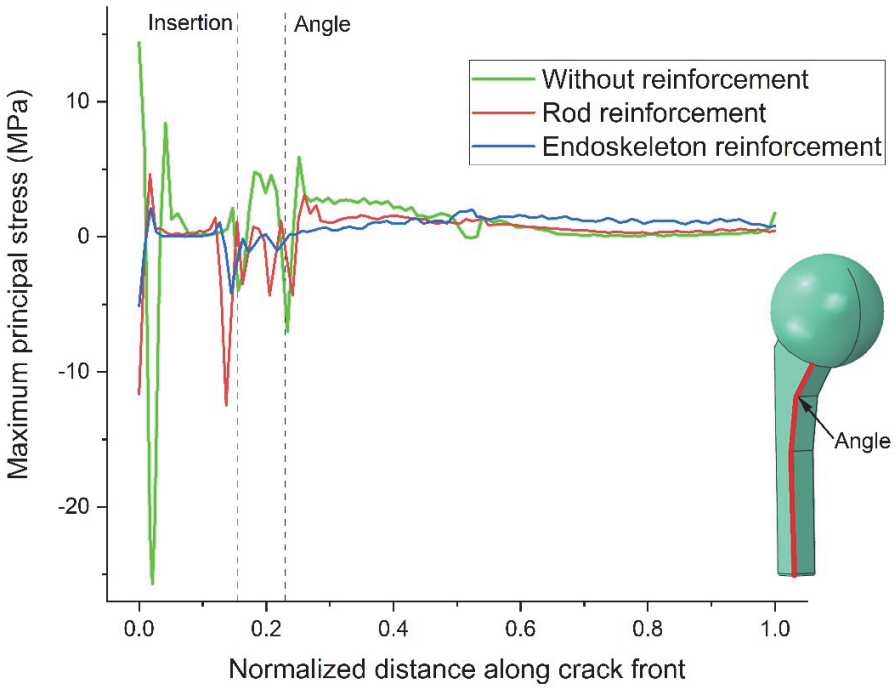

Figure 11: Distribution of maximum principal stress at the right anterior edge level of the spacer.

Distributions of the maximum principal stresses in the femur

The insertion of non-reinforced spacer generates the greatest stresses at the femur level; therefore, the values remains below the elastic limit of the cortical bone; the addition, depending on the reinforcements type, the stresses decreases with slightly different distribution behavior. Hence, the rod reinforcement allowing a more regular distribution, especially at the level of the proximal end (Fig 12).The insertion of a prosthesis contributes in the stresses reduction at the upper part level of the bone (the prosthesis transmits it directly to the lower part), which presents the phenomenon of "stress shilding"; the subjected bone part to a very small stress reduces the fracture or a second loosening risks[24,25].Particularly, adding a full-stem reinforcement increases the risk of "stress shilding".

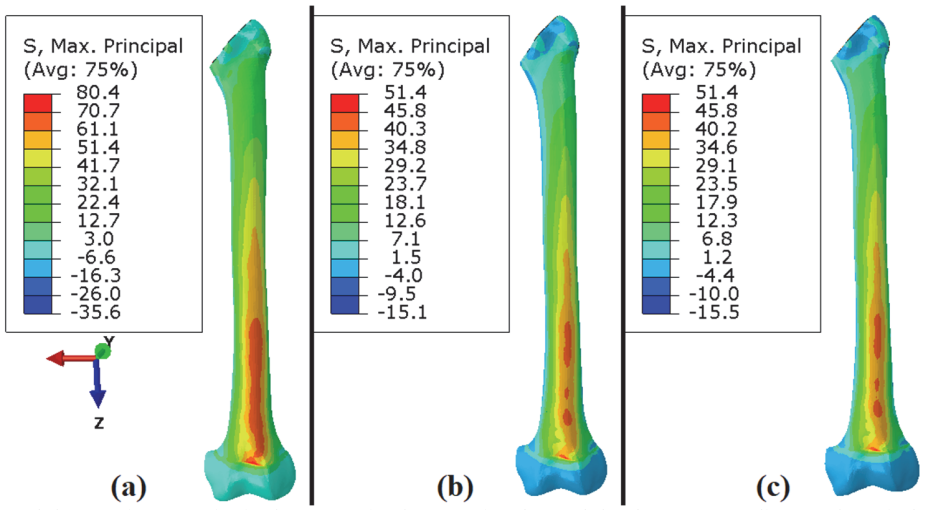

Figure 12: Distribution of the maximum principal stresses in the anterior face of the femur according to the reinforcement used. (a) without reinforcement, (b) rod reinforcement, (c) full-stem reinforcement.

Von Mises stress distribution in the reinforcements

For the assessment of the mechanical behavior of the titanium reinforcement, we compared the distribution of the equivalent von Mises stress, which is based on the plasticity criterion considered as the best method to predict the permanent deformation of metals [17]. Fig. 13 shows that, the maximum of von Mises stress in the rod reinforcement is 39% higher than the full-stem reinforcement. Regardless of the reinforcement type, this maximum equivalent stress is located at the angle of the front face level; this zone is highly solicited in compression. In the case of rod reinforcement, the stress exceeds the elastic limit (325 MPa) of titanium grade 2 studied experimentally [26].

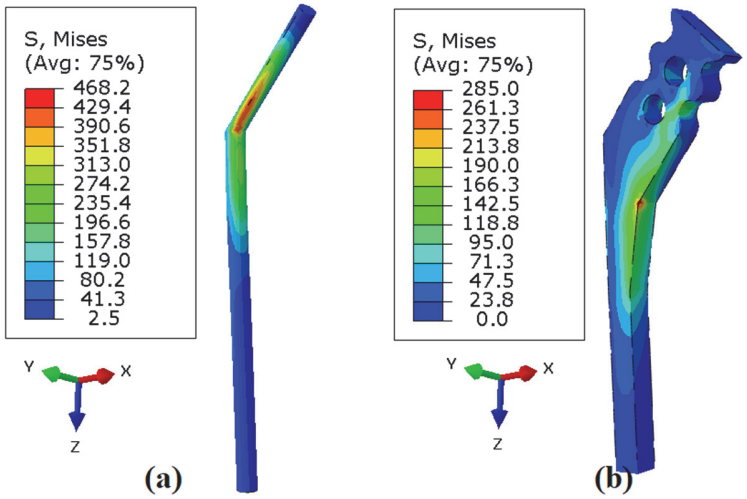

Figure 13: Distribution of von Mises stress in the reinforcement (anterior face) (a) round reinforcement 5mm in diameter, (b) full-stem reinforcement 8mm of thickness

XFEM and Fracture results

The extended finite element method (XFEM) is a relatively new modelling technique, which give us the ability to simulate the initiation and the propagation of a crack along an arbitrary trajectory [25]; hence, XFEM approach has been used recently to simulate the initiation and propagation of cracks in the field of biomechanics. Fig. 14 shows that, the predicted crack site of occurrence and trajectory by the XFEM method resembles the real crack [6, 27].

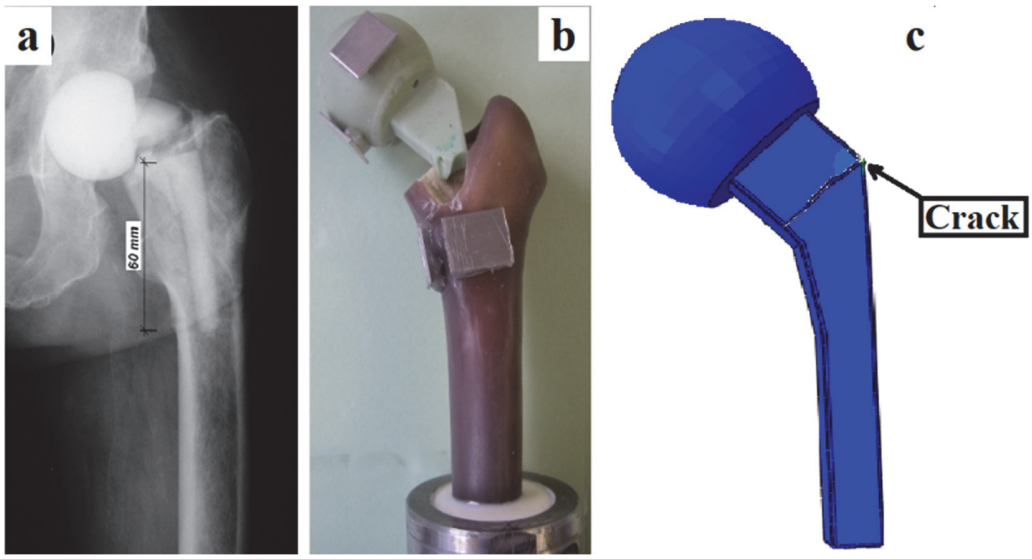

Figure 14: Cement fracture of non-reinforced spacer: a) in vivo implanted spacer radiography illustrating stem fracture [27]. b) Experimental in vitro study of fractured spacer [6]. c) Propagation crack in the cement spacer by X-FEM method.

The crack initiation following the XFEM method is situated at the left posterior edge level near the angle of the insertion into the bone (Fig. 15); consequently, the crack propagates towards both sides but precisely towards the left lateral face.

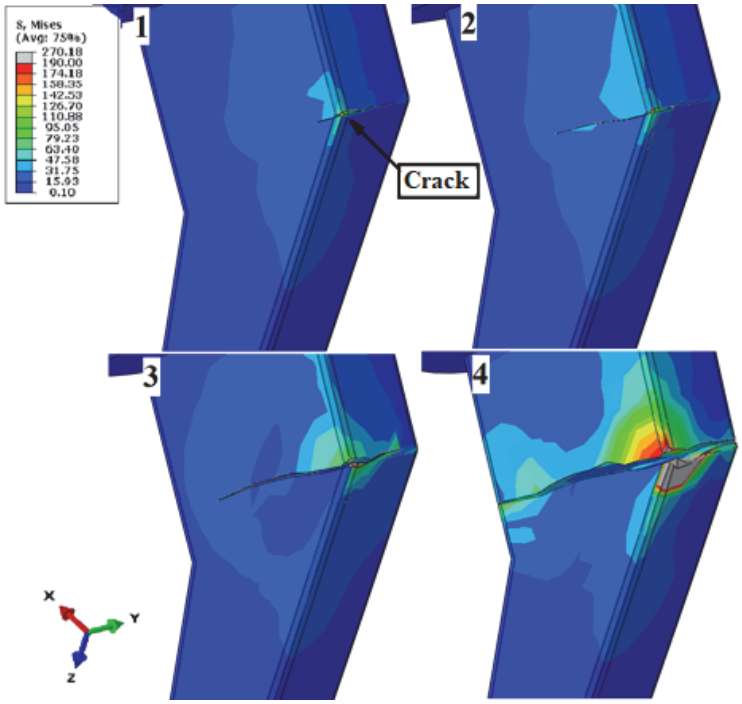

Figure 15: Crack propagation steps of the XFEM model

Stress intensity factor

The spacer without reinforcement is the most fragile, thus the distribution of the stress intensity factor will be studied in more detail. The obtained results from stress distribution investigation show that, the left posterior edge is more intensively solicited, as a result, the fracture damage of the orthopaedic cement is likely in this zone which was confirmed by the XFEM rupture model. Based on this finding, the analysis of the semi-elliptical crack behaviour initiated in the implant was performed. The convergence of the simulation with a crack radius c = 0.2mm was achieved.

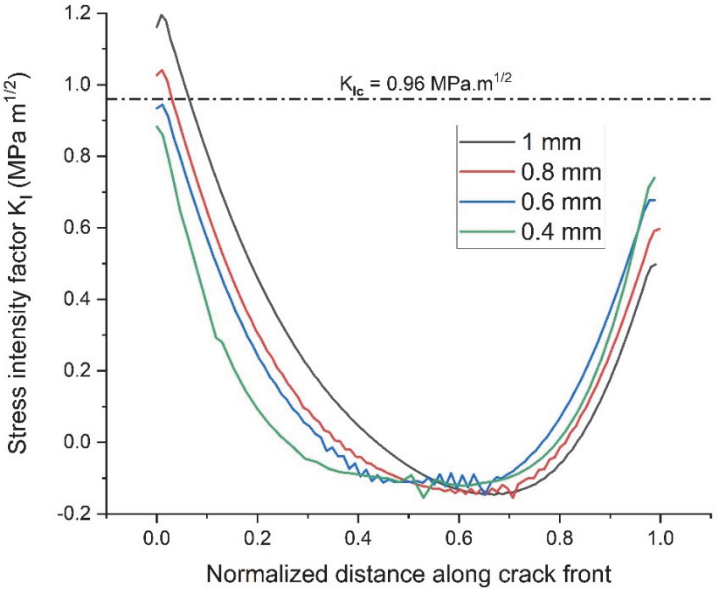

Figure 16: Stress Intensity Factor (K_I) along the crack in the PMMA bone cement

The results show that, the stress intensity factor K_I varies parabolically along the semi-elliptical crack (Fig. 16) with a minimum value located in the middle of the crack and a maximum near the two extremities. Thus, the crack extremity of the left edge side gives the highest values, with a stress intensity factor exceeding the critical value. The fracture toughness values for bone cement have been derived from tests using different sample configurations and different mixing methods ranging from 0.96 to 1.76 MPa $m^{1/2}$ [28].

The stress intensity factor increases proportionally to crack width; therefore, only crack size of 0.8 and 1 mm of half-width exceeds the tenacity value, thus leading to crack propagation towards the left face of the spacer. The found results consolidates the crack propagation tendency using XFEM approach (Fig. 15).The variation of the stress intensity factor in mode II (Fig. 17) behave similarly as mode I with much lower values, which indicates that the crack propagates mainly in mode I. Regarding mode III, the variation behaviour of the stress intensity factor changes completely and the largest values are located at the left quarter of the crack (Fig. 18), but the maximum values remain close to K_{II}.

The assessment of the stress intensity factors variation shows that, regardless the reinforcement types, the maximum values of K_I, K_{II} and K_{III} increase proportionally with crack width (Figs19-21). The maximum value was reduced by 10 to 75% using a rod reinforcement and more than 80% for the case of a full-stem reinforcement.

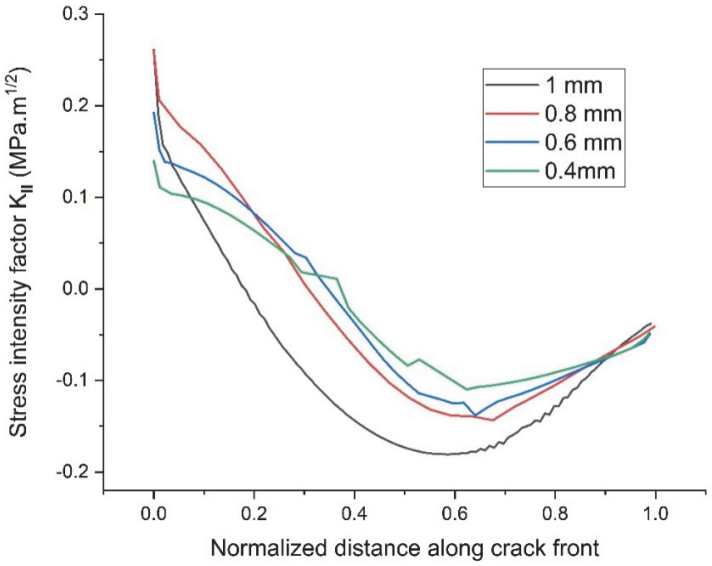

Figure 17: Stress Intensity Factor (K_{II}) along the crack in the PMMA bone cement

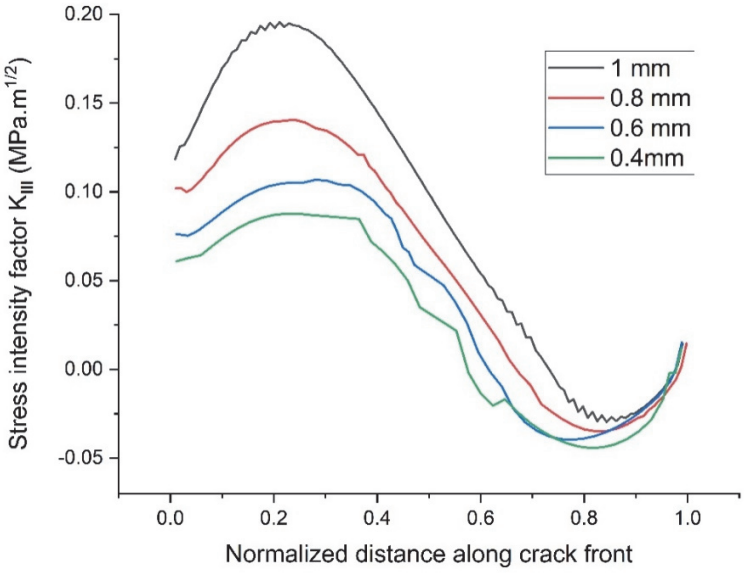

Figure 18: Stress Intensity Factor (K_{III}) along the crack in the PMMA bone cement

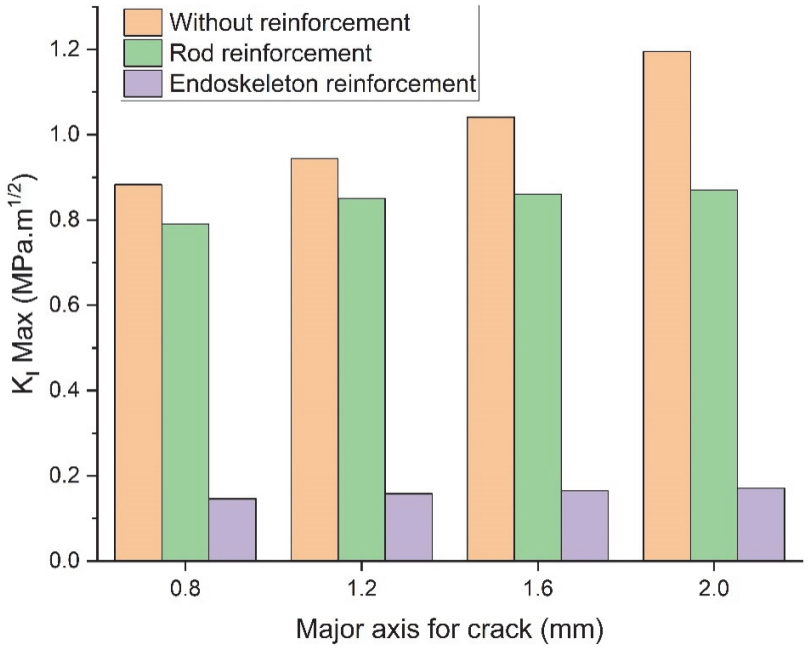

Figure 19: Comparison of maximum stress intensity factor Mode I as a function of crack length and reinforcement type.

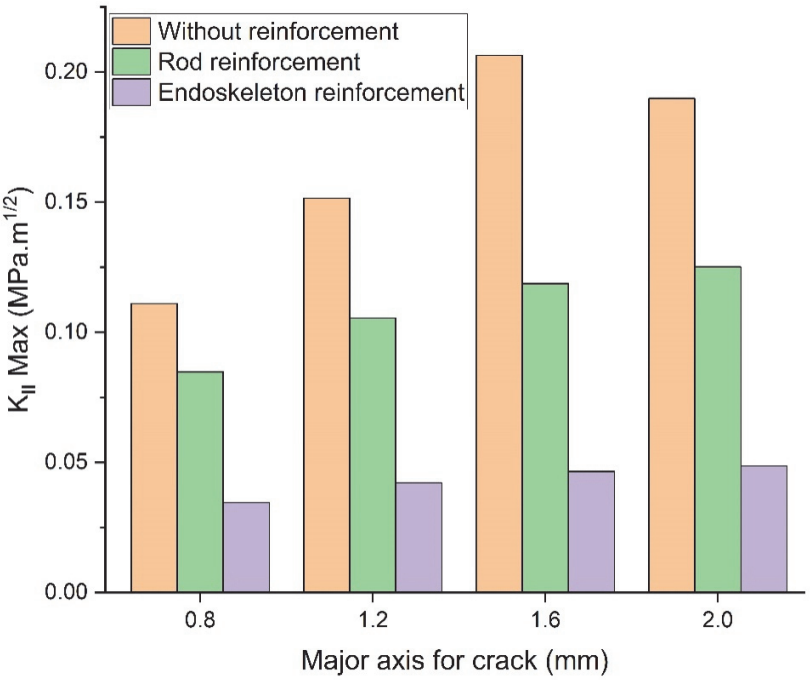

Figure 20: Comparison of maximum stress intensity factor Mode II as a function of crack length and reinforcement type.

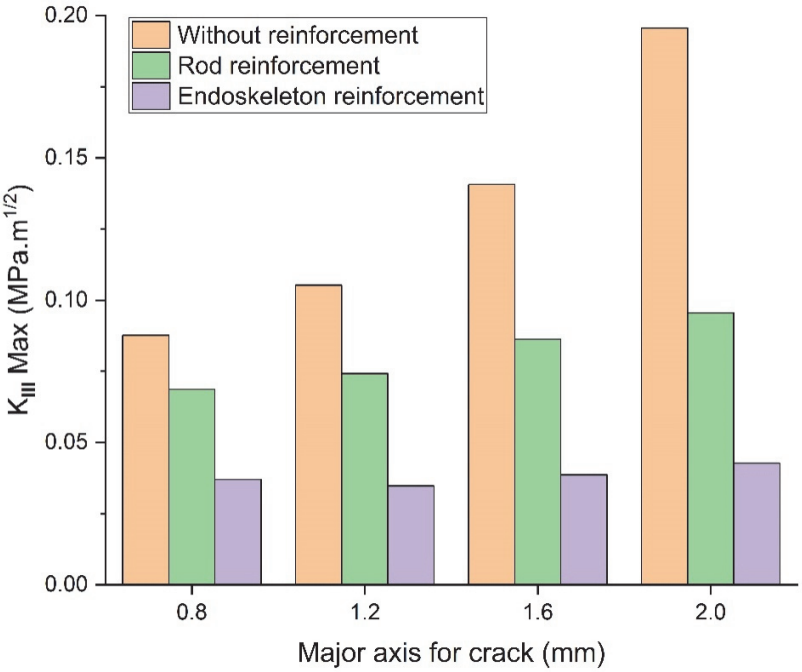

Figure 21: Comparison of maximum stress intensity factor Mode III as a function of crack length and reinforcement type.

Conclusion

The spacer is a temporary prosthesis made of orthopedic cement and enriched with antibiotics for the treatment of total hip replacement infections. Due to fragile behavior of PMMA, the spacer fractures lead to a serious problem under minimal loads. This work focuses on the fracture behavior investigation of a non-reinforced spacer and hip spacer reinforced with different reinforcements, by the calculation of principal and von Mises stresses and the stress intensity factors for cracked bone cement. The obtained results allow us to deduce the following conclusions:

- The maximum stresses are localized at the neck level of the prosthesis, as a consequence of axis offset between implant and applied force to the prosthetic head.
- Titanium reinforcement improves considerably the spacer mechanical performance by reducing the maximum tensile stress at the neck level; moreover, full-stem reinforcement avoids the exceeding of rupture stress under tensile loading of PMMA.
- Stress intensity factor analysis shows that, cracks width larger than 0.8mm encourage the crack propagation under static loading. The use of full-stem reinforcement of 8mm thickness reduce significantly the stress intensity factor and consequently prevent effectively the spacer fracture.

However, the study was carried out on a limited number of reinforcements to analyze the most effective one; therefore, in the future works will be focus on the optimization of the shape and the materials of the reinforcement which could lead to a better choice. In addition, the use of a cyclic loading will make it possible to better simulate the behavior in-vivo basing on XFEM rupture criterion.

References

[1] Zardi, E. M. and Franceschi, F. (2020). Prosthetic joint infection. A relevant public health issue. Journal of infection and public health, 12-13, pp. 1888-1891.

[2] Lieberman, J.R., Callaway, G.H., Salvati, E., Pellicci, P.M., Brause, B.D. (1994). Treatment of infected total hip arthroplasty with a two stage reimplantation protocol. Clin Orthrop., 301, pp. 205–12.

[3] Windsor, R.E., Insall, J.N., Urs, W.K., Miller, D.V., Brause, B.D. (1990). Two stage reimplantation for the salvage of total knee arthroplasty complicated by infection, Further follow-up and refinement of indications. J Bone Joint Surg Am 72, pp. 272–278.
[4] Thomas, T., Stefan, M., Arno, Z., Danièle, W. and Jens, K. (2009). Mechanical properties of PMMA for medical application. Materials testing: 51-5, pp. 203-209.
[5] Thielen, T., Maas, S., Zuerbes, A., Waldmann, D., Anagnostakos, Kelm, J. (2009). Development of a reinforced PMMA based hip spacer adapted to patients' needs. Medical Engineering & Physics. 31, pp. 930-936.
[6] Thielen, T., Maas, S., Zuerbes, A., Waldmann, D., Anagnostakos, Kelm, J. (2009). Mechanical behaviour of standardized, endoskeleton-including hip spacers implanted into composite femurs. Int J Med Sci. 6(5), pp. 280-286.
[7] Bouziane, M.M., H. Salah, S. Benbarek, BelAbbès Bachir Bouiadjra, and B. Serier. (2015). Finite Element Analysis of the Mechanical Behaviourof a Reinforced PMMA-Based Hip Spacer, Advanced Materials Research 1105, pp. 36–40.
[8] Salah, H., Bouziane, M.M., Fekih S.M., Bachir Boudjra, B., Benbarek, S. (2018). Optimization of a Reinforced Cement Spacer in Total Hip Arthroplasty. Journal of Biomimetic, Biomaterials and Biomedical Engineering. 35, pp. 35-49.
[9] Mallek, A., Miloudi, A., Khaldi, M., Bouziane, M.M., Bachir Bouiadjra, B., Bougherara, H, Gill, R.H.S. (2021). Quasi-static analysis of hip cement spacers. journal of the mechanical behavior of biomedical materials 116, 104334.
[10] Abaqus documentation (2018).
[11] Bergmann, G., Deuretzbacherb, G., Hellerc, M., Graichena, F., Rohlmanna, A., Straussb, J., Dudac, G.N., Bergmann, G et al. (2001), Hip contact forces and gait patterns from routine activities. Journal of biomechanics 34-37, pp. 859-871.
[12] [12] Duda, G. N., Heller, M., Albinger, J., Schulz, O., Schneider, E. and Claes, L. (1998). Influence of muscle forces on femoral strain distribution. Journal of biomechanics, 31(9), pp. 841-846.
[13] Nuño, N., Amabili, M., Groppetti, R., Rossi, A., (2001). Static coefficient of friction between Ti-6Al-4V and PMMA for cemented hip and knee implants,Journal of Biomedical Materials Research, 59(1), pp. 191-200.
[14] Moës, N., Dolbow, J. E., and Belytschko, T. (1999). A finite element method for crack growth without remeshing. International Journal for Numerical Methods in Engineering, 46(1), pp. 131–150.
[15] Song, J.-H., Areias, P.M.A. and Belytschko, T. (2006). A method for dynamic crack and shear band propagation with phantom nodes. Int. J. Numer. Meth. Engng., 67, pp. : 868-893.
[16] Remmers, J. J. C., De Borst, R. D., and Needleman, A. (2003). A cohesive segments method for the simulation of crack growth. Computational Mechanics, 31(1-2), pp. 69–77.
[17] Khan, A.J., Iqbal, N., Saeed, H.A., Tarar, W.A., (2016). Development of material model for assessment of brittle cracking behavior of Plexiglas. IOP Conf. Ser., Mater. Sci. Eng., 146, 012008.
[18] May-Pata, A., Herrera-Kao, W., Cauich-Rodríguez, J.V., Cervantes-U, J.M., Flores-Gallardo, S.G. (2012). Comparative study on the mechanical and fracture properties of acrylic bone cements prepared with monomers containing amine groups. J MechBehav Biomed Mater. 6, pp. 95-105.
[19] Qian, G., González-Albuixech, V. F., Niffenegger, M., &Giner, E. (2016). Comparison of KI calculation methods. Engineering Fracture Mechanics, 156, pp. 52-67.
[20] Shih, C.F., Asaro, R.J. (1988). Elastic-Plastic Analysis of Cracks on Bimaterial Interfaces: Part I-Small ScaleYielding. Journal of Applied Mechanics 55, pp. 299-316.
[21] Love, A. E. H., (1927). A Treatise on the Mathematical Theory of Elasticity, Fourth Edition. Cambridge: The University Press.
[22] Leckie, F.A., Bello, D.J.D. (2009). Failure Criteria. In: Strength and Stiffness of Engineering Systems. Mechanical Engineering Series. Springer, Boston, MA., DOI: 10.1007/978-0-387-49474-6_9.
[23] Khellafi, H., Bouziane, M. M., Djebli, A., Mankour, A., Bendouba, M., Bachir Bouiadjra, B. A., and Ould Chikh, E. B. (2019). Investigation of Mechanical Behaviour of the Bone Cement (PMMA) under Combined Shear and Compression Loading. Journal of Biomimetics, Biomaterials and Biomedical Engineering, 41, pp. 37–48.
[24] Bugbee, W.D., Sychterz, C.J., Engh, C.A. (1996). Bone remodeling around cementless hip implants. South Med J. 89, pp. 1036-1040.
[25] Niinimäki, T., Junila, J., Jalovaara, P. (2001). A proximal fixed anatomic femoral stem reduces stress shielding. International Orthopaedics. 25, pp. 85–88.
[26] Libin, Z., Jie, Z., Jianyu, Z., Zhanli, L., Ning, H. (2016). XFEM simulation of delamination in composite laminates, Composites Part A: Applied Science and Manufacturing, 80, pp. 61-71.
[27] Botchu, R., Anwar, R., Ravikumar, K.J. (2009). Fractured cement spacers-a report of two cases. Iowa Orthop J. 29, pp. 17–18.

[28] Baleani, M, Traina, F, Toni, A. (2003). The mechanical behaviour of a pre-formed hip spacer. HIP International. 13(3), pp. 159-162.
[29] Dugdale, D.S. (1960). Yielding of steel sheets containing slits. J. Mech. Phys. Solids 8, pp. 100-104.
[30] Lemaitre, J., (1985). A continuous damage mechanics model for ductile fracture. Trans. ASME, J. Eng. Mater. Technol. 107, pp. 83-89.